

ECHELLE SPECTROSCOPY OF INTERSTELLAR ABSORPTION TOWARD μ COLUMBAE WITH THE GODDARD HIGH RESOLUTION SPECTROGRAPH

J. C. BRANDT,¹ S. R. HEAP,² E. A. BEAVER,³ A. BOGGESS,⁴ K. G. CARPENTER,² D. C. EBBETS,⁵ J. B. HUTCHINGS,⁶ M. JURA,⁷
D. S. LECKRONE,² J. L. LINSKY,⁸ S. P. MARAN,⁹ B. D. SAVAGE,¹⁰ A. M. SMITH,² L. M. TRAFTON,¹¹ F. M. WALTER,¹²
R. J. WEYMANN,¹³ J. C. HOWK,¹⁰ M. SNOW,¹ T. B. AKE,¹⁴ AND K. R. SEMBACH¹⁵

Received 1998 May 8; accepted 1998 October 6

ABSTRACT

Goddard High Resolution Spectrograph echelle-mode observations of the interstellar absorption lines of Mg II, Si IV, C IV, and N V toward μ Columbae (HD 38666) are presented. The observations have a spectral resolution of 3.5 km s^{-1} and signal-to-noise ratios (S/Ns) of 20–200. The μ Col sight line ($l = 237^\circ.3$, $b = -27^\circ.1$, $d = 0.40 \text{ kpc}$, $z = -0.18 \text{ kpc}$) extends through the Local Bubble and the warm neutral, warm ionized, and hot ionized phases of the interstellar medium (ISM). The high-ionization column densities toward μ Col are $\log N(\text{Si IV}) = 12.16 \pm 0.05$, $\log N(\text{C IV}) = 12.88 \pm 0.02$, and $\log N(\text{N V}) = 11.8\text{--}12.3$. Profile fits to *Copernicus* satellite measures of O VI absorption toward μ Col yield $\log N(\text{O VI}) = 13.82 \pm 0.01$ and $b = 38.7 \text{ km s}^{-1}$. This implies $N(\text{C IV})/N(\text{O VI}) = 0.11 \pm 0.01$, which is typical of the values found for the hot ISM of the Galactic disk. The O VI profile is twice as broad as the C IV and N V profiles, even though these species have roughly similar average velocities. Some of the C IV, N V, and O VI absorption toward μ Col may occur at the interface of the Local Cloud and Local Bubble, although additional contributions to these ions probably also occur in more distant gas along the sight line. A substantial part of the Si IV absorption likely arises in warm photoionized gas in an H II region surrounding μ Col. The profile width differences among the high-ionization lines of C IV, N V, and O VI could be produced if the line of sight passes through a highly evolved supernova remnant. The observations for μ Col and for other stars observed at high resolution with the GHRS reveal that multiple gas types (warm and hot) contribute to the absorption by the highly ionized atoms along both nearby and distant sight lines. Disentangling the relative contributions from the different gas types requires high-resolution and high-S/N observations. The Mg II observations, combined with a solar Mg reference abundance, imply that the Mg depletion toward μ Col is -0.31 dex . As observed for other sight lines through the warm neutral medium, the gas-phase observations of Mg, when combined with results for Fe and Si, suggest that Mg and Fe are more deficient from the gas phase than one would expect if these elements are only contained in silicate dust grains.

Key words: ISM: abundances — ISM: general — stars: abundances

1. INTRODUCTION

During 6 years of operation aboard the *Hubble Space Telescope* (HST), the Goddard High Resolution Spectrograph (GHRS) produced important science results for a wide variety of astrophysical problems, ranging from very accurate measurements of the D/H ratio in the local interstellar medium (ISM) (Linsky et al. 1993, 1995) to the dis-

covery of an unexpected excess in the number density of low-redshift intergalactic H I clouds (Morris et al. 1991). The GHRS was designed to provide high spectral, spatial, and temporal resolution over the wavelength range from 1150 to 3200 Å with high photometric precision. Many of the scientific achievements of GHRS investigations are summarized by Brandt et al. (1994). The orbital per-

¹ Laboratory for Atmospheric and Space Physics, Campus Box 392, University of Colorado, Boulder, CO 80309-0392; brandt@lyrae.colorado.edu, snow@lyrae.colorado.edu.

² Laboratory for Astronomy and Solar Physics, Code 681, NASA Goddard Space Flight Center, Greenbelt, MD 20771; hrsheap@hrs.gsfc.nasa.gov, carpenter@stars.gsfc.nasa.gov, hrsleckrone@hrs.gsfc.nasa.gov, hrsmith@hrs.gsfc.nasa.gov.

³ Center for Astrophysics and Space Sciences, 9500 Gilman Drive, Code 011, University of California at San Diego, La Jolla, CA 92093-0111; ebeaver@ucsd.edu.

⁴ Postal address: 2420 Balsam Drive, Boulder, CO 80304; boggress@lyrae.colorado.edu.

⁵ Ball Aerospace and Technologies Corporation, P.O. Box 1062, AR1, Boulder, CO 80306; debbets@ball.com.

⁶ Dominion Astrophysical Observatory, 5071 West Saanich Road, Victoria, BC V8X 4M6, Canada; hutchings@dao.nrc.ca.

⁷ Department of Physics and Astronomy, UCLA, Los Angeles, CA 90095-1562; jura@clotho.astro.ucla.edu.

⁸ JILA, University of Colorado and National Institute of Standards and Technology, Boulder, CO 80309-0440; jlinsky@jila.colorado.edu.

⁹ Space Sciences Directorate, Code 680, NASA Goddard Space Flight Center, Greenbelt, MD 20771; hrsmaran@hrs.gsfc.nasa.gov.

¹⁰ Department of Astronomy, University of Wisconsin at Madison, 475 North Charter Street, Madison, WI 53706-1582; savage@astro.wisc.edu, howk@astro.wisc.edu.

¹¹ McDonald Observatory and Department of Astronomy, University of Texas, Austin, TX 78712; lmt@astro.as.utexas.edu.

¹² Department of Earth and Space Sciences, State University of New York at Stony Brook, Stony Brook, NY 11794-2100; fwalter@cmail.sunysb.edu.

¹³ Observatories of the Carnegie Institution of Washington, 813 Santa Barbara Street, Pasadena, CA 91101-1292; rjw@ociw.edu.

¹⁴ Science Programs, Computer Sciences Corporation, NASA Goddard Space Flight Center, Greenbelt, MD 20771; hrsake@hrs.gsfc.nasa.gov.

¹⁵ Department of Physics and Astronomy, Johns Hopkins University, 3400 North Charles Street, Baltimore, MD 21218; sembach@sundoggie.pha.jhu.edu.

formance characteristics of the GHRS are discussed by Heap et al. (1995) and Robinson et al. (1998). GHRS results related to studies of the ISM are reviewed by Savage & Sembach (1996).

When developing the Guaranteed Time Observing (GTO) program, the GHRS Investigation Definition Team agreed to pursue a number of “team projects” that would emphasize the scientific capabilities of the GHRS and produce important data sets for studying specific astrophysical problems. The GHRS team project papers so far published include (1) a survey of absorption lines in the spectrum of 3C 273 (Brandt et al. 1993), (2) a study of the UV chromospheric emission and photospheric absorption lines in α Orionis (Brandt et al. 1995), (3) observations of weak ISM absorption lines in the spectrum of ζ Ophiuchi (Brandt et al. 1996), (4) an extension of the 3C 273 survey of absorption lines (Brandt et al. 1997), (5) a survey of the numerous photospheric absorption lines in the spectrum of the narrow-line O star 10 Lacertae (Brandt et al. 1998a), and (6) an echelle atlas of the ultrasharp, chemically peculiar star χ Lupi (Brandt et al. 1998b).

In this paper, we present GHRS echelle-mode observations of interstellar absorption due to N v, C iv, Si iv, and Mg ii along the line of sight toward μ Columbae (HD 38666). The data have high enough spectral resolution ($R = \lambda/\Delta\lambda = 85,000$; $\text{FWHM} \approx 3.5 \text{ km s}^{-1}$) to resolve fully the absorption produced by the highly ionized interstellar atoms. High-resolution observations of the highly ionized ISM exist for only a few other sight lines, including γ^2 Velorum (Fitzpatrick & Spitzer 1994), HD 93521 (Spitzer & Fitzpatrick 1992), HD 167756 (Savage, Sembach, & Cardelli 1994), ζ Ophiuchi (Sembach, Savage, & Jenkins 1994), HD 217533 (Fitzpatrick & Spitzer 1997), and HD 119608 (Sembach, Savage, & Tripp 1997).

The absorption lines of highly ionized atoms provide information about the warm photoionized and hot collisionally ionized phases of the ISM. The high spectral resolution of the GHRS allows one to discriminate between the different ionization mechanisms within this gas through detailed profile comparisons. For example, Savage et al. (1994) identified two types of gas that are responsible for the complex profiles of Si iv, C iv, and N v produced along the 4 kpc path toward the halo star HD 167756. One type of gas

is hot ($T > 2 \times 10^5 \text{ K}$) and produces strong, broad C iv and N v absorption, while the other type of gas is cooler and produces most of the Si iv and some of the C iv absorption. Observations of the halo star HD 215733 by Fitzpatrick & Spitzer (1997) also reveal a complex, highly ionized medium with various mixtures of the three highly ionized species accessible to the GHRS. Our observations of μ Col were designed to provide information complementary to these previous investigations and to demonstrate the scientific usefulness of high-resolution investigations of the highly ionized ISM. For general reviews of the hot and highly ionized phases of interstellar gas, see Savage (1987) and Spitzer (1990).

This paper is organized as follows. In § 2, we provide information about the general aspects of the μ Col sight line. In § 3, we discuss the GHRS observations and data reduction procedures. Section 4 is a discussion of the interstellar measurement techniques. Section 5 contains the scientific results for the sight line to μ Col. A discussion of this work and a comparison with the results for other interstellar sight lines is presented in § 6.

2. THE μ COLUMBAE SIGHT LINE

The stellar and interstellar properties of the μ Col sight line are summarized in Table 1; μ Col is a runaway O9.5 V star with a small interstellar reddening [$E(B-V) = 0.02$] and a distance based on *Hipparcos* astrometry of 400 (100, -70) pc (ESA 1997). The sight line samples gas out to a distance of 180 pc from the Galactic plane in the direction $l = 237^\circ.3$, $b = -27^\circ.1$. The H i column density of $\log N(\text{H i}) = 19.85$ (Bohlin, Savage, & Drake 1978) implies an average H i density of $n(\text{H i}) = 0.057 \text{ cm}^{-3}$ along the sight line. H i 21 cm emission and *IRAS* 100 μm dust emission at the latitude of μ Col have a local minima extending from $l = 210^\circ$ to 240° (see Fig. 5d of Snowden et al. 1997 and Figs. 11a and 11b of Brown, Hartmann, & Burton 1995). This is a low-density sight line with no obvious large-scale interstellar structures.

Observations of μ Col with the *Copernicus* satellite (York 1974; Shull & York 1977) reveal strong interstellar O vi absorption toward μ Col, implying the presence of hot gas ($T \sim 3 \times 10^5 \text{ K}$) along the sight line. The hot gas seen in O vi absorption may be related to the modest 0.25 keV

TABLE 1
GHRS POST-COSTAR ECHELLE-A OBSERVATIONS OF μ COLUMBAE

Wavelength Range (Å)	HST ID	Aperture	Exposure Time ^a	Scattered Light d -Coefficient	Species Observed
1237–1244	Z2AZ010CT	LSA	1022.7 ^b	0.049	N v, Mg ii
	Z2AZ010OT	SSA	1022.7 ^b	0.049	N v, Mg ii
1392–1400	Z2AF010HT	LSA	25.6	0.037	Si iv
	Z2C0020HP	LSA	25.6	0.037	Si iv
1398–1405	Z2AZ010ET	LSA	1022.7 ^b	0.037	Si iv
	Z2AZ010QT	SSA	1022.7 ^b	0.037	Si iv
1398–1405	Z2AF0110T	LSA	25.6	0.037	Si iv
	Z2AF0214T	SSA	25.6	0.037	Si iv
	Z2C0030HT	LSA	25.6	0.037	Si iv
1540–1549	Z2AZ010GT	LSA	2045.4 ^b	0.031	C iv
	Z2AZ010ST	SSA	2045.4 ^b	0.031	C iv
1547–1555	Z2AF010CT	LSA	102.3	0.031	C iv
	Z2C0020CP	LSA	51.1	0.031	C iv

^a On-spectrum exposure time in seconds. The listed values are 94% of the total exposure time required for the observation. The remaining 6% was used to sample the detector background levels between the echelle orders.

^b These observations were obtained using the FP-SPLIT = 4 observing mode in order to reduce the effects of fixed pattern noise.

X-ray emission enhancement in this region of the sky, which is evident in the *ROSAT* diffuse X-ray survey maps presented by Snowden et al. (1997; see their Fig. 2).

Extensive analyses and results have been published for the properties of the warm neutral ISM along the μ Col sight line. Shull & York (1977) provided a complete analysis of *Copernicus* satellite spectra of various far-ultraviolet absorption lines, while Sofia, Savage, & Cardelli (1993) reported on a GHRs program designed to obtain information about gas-phase elemental abundances in the neutral clouds along the line of sight.

3. OBSERVATIONS AND DATA REDUCTION

The GHRs echelle-mode observations of μ Col listed in Table 1 were obtained in 1994 March and April as part of *HST* programs GTO 5540, 5592, and 5593 (the principal investigator was D. Ebbets). The various entries include the wavelength coverage of the integration, the *HST* archive identification for the spectrum, the science aperture used, the on-spectrum integration time in seconds, the scattered light correction coefficient (see below), and the various ISM species observed. The measurements were obtained for the dual purpose of evaluating the post-COSTAR performance of the GHRs and for investigating the interstellar absorption along the line of sight. The various integrations were obtained with the light of the star in either the large or small science apertures, as indicated in Table 1. Standard on-board target acquisition procedures were followed. In all cases, substep pattern 7 was used for data acquisition with the 500 channel diode array of the Digicon detector. This scan pattern provides four observation substeps per diode and samples the interorder background to each side of the object spectrum with the full diode array. Approximately 94% of the total integration time was spent on the object spectrum, and the remaining 6% was spent on the interorder background. For the observations with long integration times (> 1000 s), the spectra were obtained using a fixed pattern split observing mode (FP-SPLIT = 4) in order to reduce the effects of fixed pattern noise in the spectra that is due to the detector and photocathode granularity.

We used the standard GHRs software available at the Goddard Space Flight Center to extract the data, apply paired pulse corrections, subtract the interorder background, and assign wavelengths. The echelle-mode scattered light d -coefficients from Cardelli, Ebbets, & Savage (1993), adopted for each integration, are listed in Table 1. We have adopted those corrections appropriate for the small science aperture (SSA) since the scattered light coefficients in the large science aperture (LSA) are poorly characterized.

Producing the final averaged spectra required merging the different individual spectra listed in Table 1. In cases where the signal-to-noise ratio (S/N) is very high (1238–1244, 1399–1404, and 1543–1549 Å), we used the individual FP-SPLIT subexposures to solve for and remove the detector fixed pattern noise as outlined by Cardelli & Ebbets (1994). For cases where the data have lower S/Ns, we simply aligned and merged the spectra using the centroids of the interstellar lines to determine the net shifts between each subexposure.

Figure 1 contains the fully reduced spectra that was obtained through the above procedures. The net count rate (in units of counts s^{-1} diode $^{-1}$) is plotted against the LSR vacuum wavelength (in angstrom units). Adopting the solar

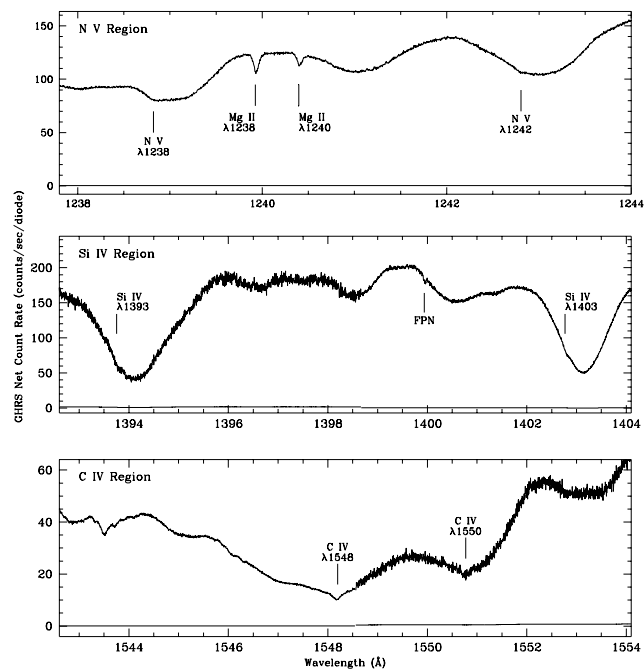


FIG. 1.—GHRs spectra of μ Col for the spectral regions containing N v (top), Si iv (middle), and C iv (bottom). In each panel, the upper curves show the GHRs net count rate (in units counts s^{-1} diode $^{-1}$) plotted against the LSR wavelength in angstrom units. The lower curves of each panel show the error spectra. The rest LSR wavelengths of the interstellar absorption lines are indicated with the vertical tick marks.

velocity and direction from Mihalas & Binney (1981), we find that toward μ Col, $v_{\text{LSR}} - v_{\text{HELIO}} = -16.5$ km s^{-1} . However, to be consistent with velocities in the existing ISM measurements in the literature (Shull & York 1977; Sofia et al. 1993), we have instead adopted for our study the correction used in those papers, $v_{\text{LSR}} - v_{\text{HELIO}} = -19.9$ km s^{-1} . The rest wavelengths of the various ISM lines are identified with tick marks. The noise spectra based on Poisson statistics are plotted underneath each data spectrum in Figure 1. These data have S/N ≈ 75 –200 per quarter diode stepped sample in the continua near the lines of N v $\lambda\lambda 1238.821, 1242.804$; Mg II $\lambda\lambda 1239.925, 1240.395$; Si iv $\lambda 1402.770$; and C iv $\lambda 1548.195$. Near the Si iv $\lambda 1393.755$ and C iv $\lambda 1550.770$ lines, the S/N is ≈ 30 and 20, respectively. A residual fixed pattern noise structure is evident near 1400 Å.

Special wavelength calibrations were not obtained as part of the μ Col data acquisition. Therefore, the final spectra have velocity uncertainties determined by the precision of the GHRs grating wheel rotation and the centering of the star in the LSA. Together, these produce an uncertainty ≈ 4.0 km s^{-1} (1σ).

4. INTERSTELLAR MEASUREMENTS

In Figure 2, we plot expanded versions of the GHRs echelle observations of the Mg II, Si iv, C iv, and N v line profiles for the μ Col sight line. The smooth solid lines represent our best estimate of the continuum for each interstellar absorption line. The continua were fitted with Legendre polynomials estimated from line-free regions on both sides of each interstellar absorption feature (see Sembach & Savage 1992). The N v continua fits are par-

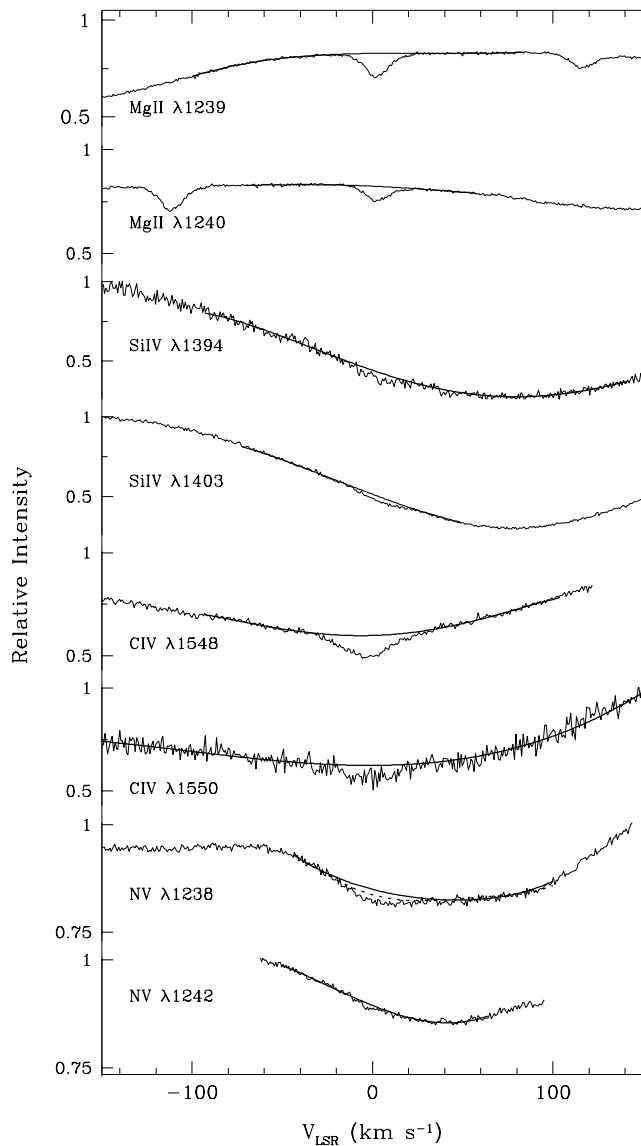


FIG. 2.—Relative intensity vs. LSR velocity for the interstellar lines observed toward μ Col by the GHRs in high-resolution ($\text{FWHM} \approx 3.5 \text{ km s}^{-1}$) mode. The smooth solid curves overplotted on the spectra are best estimates of the stellar continuum at the locations of the interstellar lines. For the $\text{N v } \lambda 1238$ line, two continuum choices are illustrated. Our preferred continuum is the solid line.

ticularly uncertain because the interstellar N v lines are weak and partially blended with stellar absorption. In Figures 2 and 3, we indicate with a dotted line a second possible continuum choice for the $\text{N v } \lambda 1238.821$ line and the resulting normalized line profile. The interstellar Si iv and C iv lines lie on relatively smooth regions of the stellar profiles for μ Col or on well-developed stellar P Cygni wind profiles for HD 119608. Therefore, the continua for these lines are relatively well determined.

Continuum-normalized versions of the line profiles in Figure 2 are shown in Figure 3. We have supplemented the data with a profile for $\text{S III } \lambda 1190.208$ from Howk, Savage, & Fabian (1998) and for $\text{O VI } \lambda 1031.926$ from York (1974). Both species provide important information about the origin of the highly ionized gas along the sight line (see § 5). The two continuum-normalized profiles shown for the N v

$\lambda 1238.821$ line reflect the two continuum choices given in Figure 2.

Total equivalent widths and errors for the interstellar lines shown in Figure 3 can be found in Table 2. The errors include statistical uncertainties and continuum placement uncertainties according to the procedures discussed by Sembach & Savage (1992). However, the continuum placement errors on the N v lines are much larger and can only be estimated approximately by evaluating plausible ranges for the continuum. The second value of the equivalent width listed for the $\text{N v } \lambda 1238.821$ line reflects the value obtained for the dashed continuum choice shown in Figure 2.

We have estimated column densities for the species shown in Figure 3 by using the apparent optical depth method. A continuum-normalized absorption profile, $I(v)$, for a line having a rest wavelength, λ (in angstrom units), and an oscillator strength, f , is related to an apparent

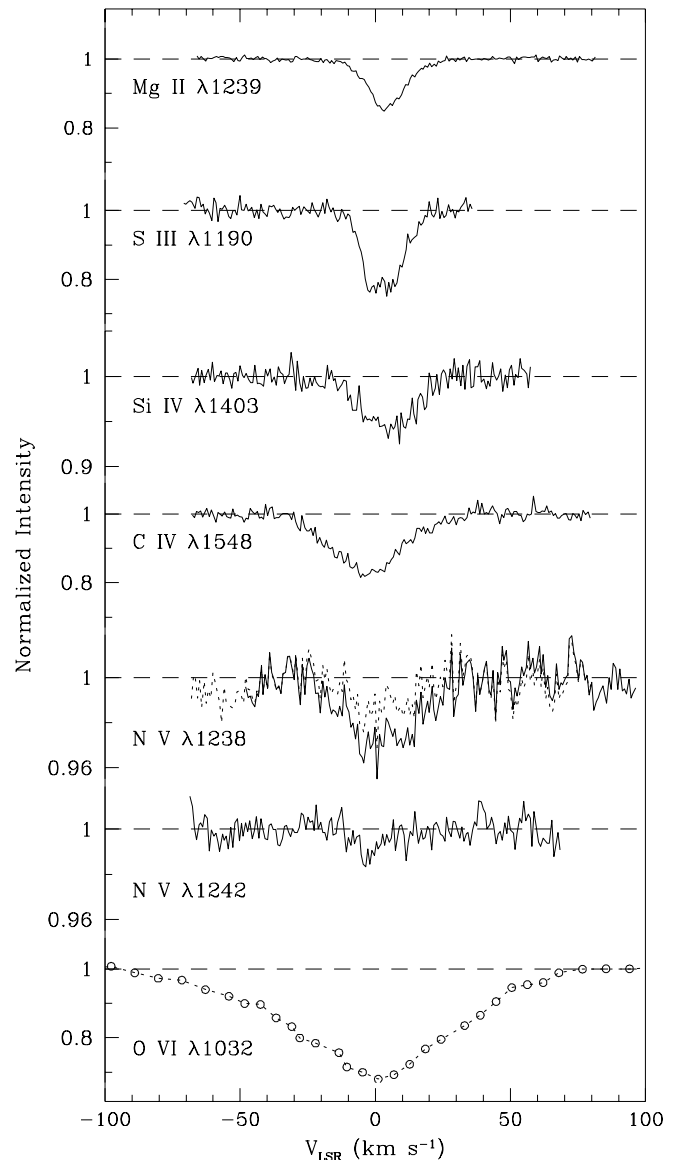


FIG. 3.—Continuum-normalized line profiles for the interstellar lines in Fig. 2 for μ Col. The solid and dashed lines for the $\text{N v } \lambda 1238$ profiles were derived from the two continuum levels shown in Fig. 2. The profiles for $\text{S III } \lambda 1190.208$ from Howk et al. (1998) and $\text{O VI } \lambda 1031.926$ from York (1974) have been added to aid the scientific interpretations.

TABLE 2
EQUIVALENT WIDTHS AND APPARENT COLUMN DENSITIES^a

Ion	λ (Å)	$W_{\lambda} \pm 1 \sigma$ (mÅ)	$\log N_a(\text{cm}^{-2}) \pm 1 \sigma$
Mg II.....	1239.925	10.6 ± 0.3	15.11 ± 0.03
	1240.395	5.83 ± 0.20	15.14 ± 0.03
S III ^b	1190.208	16.3 ± 0.6^b	13.82 ± 0.02^b
Si IV.....	1393.755	11.73 ± 2.17	12.15 ± 0.09
	1402.770	6.2 ± 0.6	12.17 ± 0.05
C IV.....	1548.198	28.7 ± 1.6	12.88 ± 0.02
	1550.770	15.3 ± 1.6	12.90 ± 0.05
N V.....	1238.821	3.9 ± 0.5^c	12.27 ± 0.06^c
	1238.821	1.3 ± 0.3^c	11.80 ± 0.10^c
	1242.804	0.65 ± 0.13^c	11.79 ± 0.10^c
O VI ^d	1031.926	81 ± 3^d	13.82 ± 0.02^d

^a The observed equivalent width, W_{λ} , and the total apparent column density, $N_a = \int N_a(v)dv$, are integrated over the full velocity range of the absorption lines. The f -values that are used to calculate N_a are from Morton 1991, except for Mg II, for which we used the f -values recommended by Fitzpatrick 1997. Errors listed include contributions from continuum placement, statistical noise fluctuations, and a 2% background uncertainty.

^b The interstellar observations for μ Col have been supplemented with an observation of S III λ 1190.208 absorption from Howk et al. 1998. The S III continuum normalized profile and $N_a(v)$ profile are shown in Figs. 3 and 4. The $N_a(v)$ profile was constructed using the S III f -value from Morton 1991.

^c The continuum levels are uncertain for the N V absorption lines, and the listed errors do not include this large systematic error. The two results listed for the stronger N V λ 1238.821 line were derived from the two choices of continuum levels shown in Fig. 2. The N V column density probably lies somewhere in the range from $\log N(\text{N V}) = 11.8$ to 12.3.

^d The interstellar observations for μ Col have been supplemented with the *Copernicus* satellite observation of O VI λ 1031.926 absorption from York 1974. The O VI continuum normalized profile and the $N_a(v)$ profile are shown in Figs. 3 and 4. The $N_a(v)$ profile was constructed using the O VI f -value from Morton 1991.

column density profile, $N_a(v)$ [in units of atoms cm^{-2} (km s^{-1})⁻¹], through the following equation:

$$N_a(v) = \frac{m_e c / \pi e^2}{f \lambda} \tau_a(v) = -3.768 \times 10^{14} \frac{\ln [I(v)]}{f \lambda(\text{Å})}. \quad (1)$$

For the high ions, $N(v) \approx N_a(v)$ since the lines are fully resolved at the GHRS resolution of 3.5 km s^{-1} , and therefore $N = \int N_a(v)dv$. Savage & Sembach (1991) have shown that the conversion specified in equation (1) results in a valid, instrumentally blurred version of the true $N(v)$ profile, provided it does not contain a significant amount of unresolved saturated structure. The total apparent column densities derived from direct integrations of the ultraviolet lines are listed in Table 2. The corresponding $N_a(v)$ profiles are shown in Figure 4. In deriving these results, we used f -values from Morton (1991), except for Mg II, for which we have adopted the recent estimates from Fitzpatrick (1997). The Mg II f -values recommended by Fitzpatrick are smaller by a factor of 1.95 than the values recently determined by Sofia, Cardelli, & Savage (1994), and they are larger by a factor of 2.6 than the theoretical determination by Hibbert et al. (1983). The $N_a(v)$ profiles are valuable since they permit direct species-to-species profile shape comparisons.

To obtain physical information about the absorption and constrain the temperature of the absorbing gas, we have determined profile fits of Doppler-broadened, single-component absorption to the Si IV, C IV, and N V GHRS observations for μ Col. Using the profile-fitting procedures

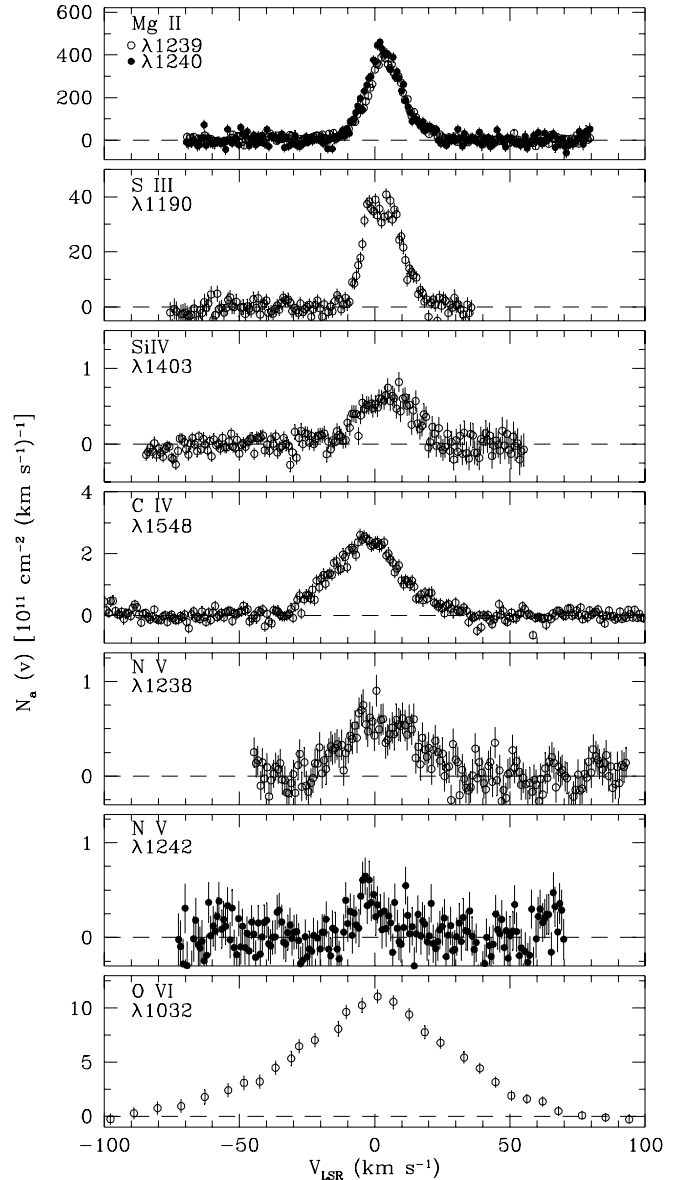


FIG. 4.—Column density per unit velocity [atoms cm^{-2} (km s^{-1})⁻¹] vs. LSR velocity for the ultraviolet interstellar line data shown in Figs. 1, 2, and 3 for μ Col.

discussed by Sembach, Danks, & Savage (1993), we obtain the following results for v_{LSR} , b , and $\log N$:

Si IV λ 1403: $v_{\text{LSR}} = 4.6 \pm 1.1 \text{ km s}^{-1}$; $b = 13.6 \pm 0.8 \text{ km s}^{-1}$; $\log N = 12.20 \pm 0.04$.

C IV λ 1548: $v_{\text{LSR}} = -3.1 \pm 0.5 \text{ km s}^{-1}$; $b = 17.9 \pm 0.4 \text{ km s}^{-1}$; $\log N = 12.88 \pm 0.01$.

N V λ 1238: $v_{\text{LSR}} = 2.7 \pm 1.8 \text{ km s}^{-1}$; $b = 17.8 \pm 1.4 \text{ km s}^{-1}$; $\log N = 12.28 \pm 0.04$.

We assumed that the instrumental blurring function for the GHRS is a Gaussian with FWHM = 3.5 km s^{-1} . The N V result assumes the higher continuum level shown in Figure 2. The velocity errors listed for Si IV, C IV, and N V are random errors associated with the fitting process and do not allow for the $\sim 4.0 \text{ km s}^{-1}$ positioning uncertainty associated with the GHRS carousel grating rotations.

Applying the same fitting process to the *Copernicus* satellite O VI λ 1032 profile from York (1974), but with a instru-

mental blurring function having FWHM = 13.5 km s⁻¹, we obtain O VI λ 1032: $v_{\text{LSR}} = -0.9 \pm 0.4$ km s⁻¹; $b = 38.7 \pm 0.3$ km s⁻¹; $\log N = 13.82 \pm 0.01$.

The O VI column density we obtain is the same as that determined by York (1974) and Shull & York (1977). The LSR velocity we obtain differs from the value $v_{\text{LSR}} = -7.4$ given by Shull & York (1977). Some of this velocity difference may come from the *Copernicus* spectrometer temperature correction to the wavelength scale discussed by Shull & York (1977; see their Appendix B).

The component fit results listed above are in good agreement with the integrals over $N_a(v)$ given in Table 2. For Si IV and C IV, the profile fits are excellent. For O VI and N V, a single-component, Doppler-broadened line provides a poor representation of the observed profile. However, the true component structure of these absorptions is not well enough constrained by the observations to warrant fitting multiple components. The component fit results for N V λ 1238 are more uncertain than the statistical errors suggest because of the systematic continuum placement difficulties.

5. RESULTS

5.1. Kinematical Properties of the Gas

The neutral and weakly ionized gas toward μ Col produces absorption in a relatively broad velocity component centered near $v_{\text{LSR}} = 3$ km s⁻¹, with additional low column density components near 21, 33, and 42 km s⁻¹ (Shull & York 1977; Sofia et al. 1993). The Mg II absorption shown in Figures 3 and 4 has a principal absorption component at 3 km s⁻¹ and weak absorption near 21 km s⁻¹. The stronger absorption lines from other ions found in H I regions confirm the reality of this weak feature and are required to see additional low column density, higher velocity absorption components (Sofia et al. 1993). The S III and Si IV absorptions are centered near 5 km s⁻¹, while the broad C IV and O VI absorptions are centered near -2 km s⁻¹. The uncertain N V absorption is centered near 2 km s⁻¹.

The various absorption profiles illustrated in Figure 3 and the $N_a(v)$ profiles in Figure 4 increase in width as the level of ionization increases. In the progression Mg II, S III, Si IV, C IV, N V, and O VI, the full widths of the $N_a(v)$ profiles in Figure 4 are approximately 14, 16, 23, 29, 29, and 63 km s⁻¹, respectively. Progressions in line width with increasing ionization stages have also been seen for other interstellar sight lines (see Sembach & Savage 1994).

5.2. Column Densities, Mean Density, and Mg Depletion

The $N_a(v)$ profiles illustrated in Figure 4 are fully resolved by the GHRS, and the lines are relatively weak [$\tau_{\text{MAX}}(\text{C IV}) \approx 0.2$ and $\tau_{\text{MAX}}(\text{Mg II}) \approx 0.3$]. Therefore, a weighted average of the values of $N_a = \int N_a(v)dv$ listed in Table 2 provides a good measure of the total column density of each species along the line of sight. We conclude that $\log N(\text{Mg II}) = 15.12 \pm 0.02$, $\log N(\text{S III}) = 12.82 \pm 0.02$, $\log N(\text{Si IV}) = 12.16 \pm 0.05$, $\log N(\text{C IV}) = 12.88 \pm 0.02$, $\log N(\text{N V}) = 11.8\text{--}12.3$, and $\log N(\text{O VI}) = 13.82 \pm 0.02$. The column density range listed for N V reflects the very large systematic uncertainty in the continuum placement shown in Figure 3.

The well-determined C IV column density, $\log N(\text{C IV}) = 12.88 \pm 0.02$, implies an average line-of-sight C IV density of $\langle n(\text{C IV}) \rangle = 6.1 \times 10^{-9}$ cm⁻³. This is slightly less than the average midplane density of C IV, $\langle n(\text{C IV}) \rangle = 9.2 \times 10^{-9}$ cm⁻³, determined for a large

number of stars situated in the Galactic disk and halo (Savage, Sembach, & Lu 1997). The highly ionized gas in the disk and low halo of the Galaxy is irregularly distributed (Sembach & Savage 1992; Savage et al. 1997); μ Col evidently lies in a Galactic direction where the highly ionized gas density is relatively close to average.

The column density of Mg II can be reliably determined along the μ Col sight line in the low-velocity gas. The value we obtain, $\log N(\text{Mg II}) = 15.12 \pm 0.02$, can be compared with the more uncertain value of 14.94 (0.26, -0.79) reported by Sofia et al. (1993). This latter result has been corrected for the change in the Mg II f -values recommended by Fitzpatrick (1997). Combining $\log N(\text{Mg II}) = 15.12 \pm 0.02$ with the value $\log N(\text{H I}) = 19.85$ and $\log N(\text{H}_2) = 15.51$ (Bohlin et al. 1978; Savage et al. 1977), we obtain $\log [N(\text{Mg II})/N(\text{H})] = -4.73$. Mg II is the dominant ionization state of Mg in the warm neutral medium. Indeed, the Mg I column density along the sight line is $\log N(\text{Mg I}) = 12.47 \pm 0.03$ (Sofia et al. 1993), which implies $N(\text{Mg II})/N(\text{Mg I}) \approx 450$. The solar abundance of Mg is $\log (\text{Mg}/\text{H})_{\odot} = -4.42$ (Anders & Grevesse 1989). The measured gas-phase Mg abundance along the sight line is lower by 0.31 dex or a factor of 2.0 compared with that found in the Sun. The incorporation of Mg into interstellar dust is the likely explanation for the subsolar abundance. However, another possibility is that the Sun is overabundant in many elements by ~ 0.3 dex (Cardelli et al. 1996; Mathis 1996; Meyer, Jura, & Cardelli 1998). The gas-phase abundance of Mg can be combined with results for Fe and Si to infer the composition of the dust. If the solar system composition is appropriate for the ISM, Sofia et al. (1994) and Fitzpatrick (1997) conclude, based on studies of a number of sight lines, that a substantial fraction of the Mg and Fe must reside in a grain population other than silicates. Using the values of $N(\text{Fe II})$ and $N(\text{Si II})$ from Sofia et al. (1993) and our new value of $N(\text{Mg II})$, along with the solar abundances adopted by Sofia et al. and the value of $N(\text{H I})$ listed above, we derive $(\text{Mg} + \text{Fe})/\text{Si} = 2.8$ in the dust in the warm neutral medium toward μ Col. For a population of silicate grains, this ratio is expected to range from 1.0 to 2.0, depending on the particular type of silicate grain. In the ISM toward μ Col, there is more Mg and Fe missing from the gas phase than can be explained by the incorporation of these elements into silicate grains alone.

5.3. Photoionized Gas

Since μ Col is an O9.5 V star, it is possible that photoionized gas in a low-density H II region surrounding the star is responsible for some of the highly ionized gas we detect. To explore this possibility, we have used the photoionization code CLOUDY (version 90.04; Ferland 1996; Ferland et al. 1998) to calculate the expected column densities of various ions that would be produced in an H II region surrounding a star with $T_{\text{eff}} = 33,000$ K and $L = 1.2 \times 10^{38}$ ergs s⁻¹ (Howarth & Prinja 1989). For the input spectrum of the central star, we have used an ATLAS (Kurucz 1991) model atmosphere with $\log g = 4.0$, which includes line blanketing but assumes LTE. The ionization balance and temperature structure of the nebula were determined from a radius of 0.03 pc to the distance where the electron density falls below 10% of the total hydrogen density. The model calculations have assumed solar abundances (Anders & Grevesse 1989). We note that CLOUDY does not include an accurate dielectronic recombination rate for Si⁺³ but rather adopts the

average rate coefficients for C, N, and O ($=2.5 \times 10^{-11} \text{ cm}^{-3} \text{ s}^{-1}$).

Since the physical conditions appropriate for an H II region surrounding μ Col are poorly constrained, we give the results for three illustrative models in Table 3. The quantities listed include the ambient density and filling factor (per volume) stipulated in the models, the radius of the H II region, and the model column densities from the star to the edge of the H II region for S III, Si IV, and C IV. The models predict negligible amounts of N V and O VI. The assumed ambient densities for these models include a value for the average sight line density (0.05 cm^{-3}) and the H II region density (0.2 cm^{-3}) estimated by Shull & York (1977) and based on their examination of the fine-structure lines of N II in *Copernicus* satellite spectra of μ Col. A lower density model (0.02 cm^{-3}) was also calculated. The three models reproduce the observed amount of S III, $\sim 60\%$ of the observed Si IV, and less than 1% of the observed C IV.

The CLOUDY models predict significantly lesser amounts of highly ionized gas than do those of Black et al. (1980) and Cowie, Taylor, & York (1981). For a uniform-density nebular model with $n = 1 \text{ cm}^{-3}$, CLOUDY models predict $\log N(\text{Si IV}) = 13.18$ and $\log N(\text{C IV}) = 11.83$, compared with $\log N(\text{Si IV}) \sim 14.4$ and $\log N(\text{C IV}) \sim 13.5$ from Cowie et al. (1981). A portion (perhaps a factor of 2–4) of this difference is provided for by the different atomic constants used in the CLOUDY code (Ferland 1996). The flux of ionizing photons in our models is approximately the same as in the Black et al. (1980) models. Whereas the earlier models have assumed constant temperature nebulae, CLOUDY follows the temperature structure of the nebula explicitly by calculating the associated changes in the atomic cross sections for each temperature zone in the nebula.

While there are many uncertainties involved, the photoionization modeling implies that the observed amount of S III and a significant fraction of the Si IV detected along the line of sight are consistent with an origin in the H II region surrounding μ Col. However, μ Col is too cool to produce appreciable amounts of C IV, N V, or O VI by photoionization.

5.4. Hot, Collisionally Ionized Gas

For discussions of various possible sites for the origin of highly ionized atoms in the ISM, see Sembach et al. (1997), Savage et al. (1997), and Spitzer (1990, 1996). The observations for μ Col are particularly significant for probing the

ionization conditions in the gas since measurements exist for a wide range of ionization states, including O VI.

The production of C IV, N V, and O VI from their lower ion states requires energies of 48, 77, and 114 eV, respectively. Since hot stars usually have strong He^+ absorption edges at 54 eV, it is unlikely that N V or O VI are produced in significant quantities by starlight photoionization. The photoionization modeling discussed in § 5.3 shows that the H II region surrounding μ Col should contain only a small amount of C IV and essentially no N V or O VI. Therefore, the origin of these three ions likely involves collisional ionization processes in the hot ISM along the sight line.

The high-ionization column density ratios toward μ Col are $N(\text{C IV})/N(\text{Si IV}) = 5.3 \pm 0.07$, $N(\text{C IV})/N(\text{N V}) = 3.8\text{--}12$, and $N(\text{C IV})/N(\text{O VI}) = 0.11 \pm 0.01$. The result for $N(\text{C IV})/N(\text{Si IV})$ is likely affected by the presence of photoionized Si IV in the H II region surrounding μ Col. If we assign 60% of the Si IV along the line of sight to the H II region as suggested by the photoionization calculations presented in Table 3, the remaining 40%, or $\log N(\text{Si IV}) \sim 11.76$, may be associated directly with the C IV absorption. This would imply $N(\text{C IV})/N(\text{Si IV}) \sim 13$ in that gas. The value for $N(\text{C IV})/N(\text{O VI})$ is similar to the average value found for six lines of sight through disk gas by Spitzer (1996).

The Si IV, C IV, N V, and O VI absorption lines toward μ Col have Doppler spread parameters derived from profile fitting of $b = 13.6, 17.9, 17.8,$ and 38.7 km s^{-1} , respectively (see § 4). Assuming the profiles are single components dominated by thermal Doppler broadening, we infer $T < 3.1 \times 10^5, 2.3 \times 10^5, 2.7 \times 10^5,$ and $1.4 \times 10^6 \text{ K}$, respectively. If kinematic flows, multiple components, or turbulence contribute to the observed line widths, then the temperatures will be less than these values. In collisional ionization equilibrium at $1.4 \times 10^6 \text{ K}$, very little O VI should be present, $n(\text{O VI})/n(\text{O}) \sim 3 \times 10^{-3}$ (Sutherland & Dopita 1993). Therefore, it is likely that the O VI profile width is dominated by gas kinematics rather than by thermal Doppler broadening. The poor representation of the O VI profile by a single Gaussian component supports this idea. The profiles for Si IV, C IV, and N V are consistent with the possibility that these three species are created by collisional ionization in gas with $T < (2\text{--}3) \times 10^5 \text{ K}$.

In collisional ionization equilibrium, Si IV, C IV, N V, and O VI peak in abundance at $0.8 \times 10^5, 1 \times 10^5, 2 \times 10^5,$ and $3 \times 10^5 \text{ K}$, respectively. However, gas in the temperature range from 10^5 to 10^6 K cools very rapidly. Therefore, the favored production mechanisms for these ions usually

TABLE 3
PHOTOIONIZATION MODELS FOR THE μ COL H II REGION

$n(\text{H})^a$ (cm^{-3})	f^b	R_s^c (pc)	$\log N(\text{S III})^d$	$\log N(\text{Si IV})^d$	$\log N(\text{C IV})^d$
0.02	0.7	275	13.79	11.90	11.04
0.05	0.5	167	13.84	11.93	10.95
0.2	0.25	84	13.84	11.95	10.67
Observed	13.82	12.16	12.88

^a The average assumed ambient density for the H II region model (in units of H atoms cm^{-3}). The models bracket the observed line-of-sight H I density of $0.057 \text{ atoms cm}^{-3}$.

^b The volume filling factor of the gas within the model H II region.

^c The outer radius of the model H II region.

^d Column densities of the indicated ions integrated through the H II region from the star to the outer H II region radius.

TABLE 4
COMPARISON OF OBSERVATIONS AND THEORY

Object	Observed μ Col	Mixing (25 km s ⁻¹)	Layers ^a (100 km s ⁻¹)	Cooling Fountain ^b	Conductive Interface ^c	SNR Bubble ^d
$N(\text{C IV})/N(\text{Si IV})$	5.3 ± 0.7^e	(7.4, 1.6)	(19, 4.5)	3.0–4.7	20–26	12–20
$N(\text{C IV})/N(\text{N V})$	3.8–12	(7.8, 9.1)	(18, 28)	2.2–6.8	1.8–2.6	1.9–2.3
$N(\text{C IV})/N(\text{O VI})$	0.11 ± 0.01	(1.0, 1.2)	(2.2, 3.4)	0.1–0.5	0.2–0.4	0.1–0.2

^a TML model results from Slavin, Shull, & Begelman 1993 for two values of v_e , the hot gas entrainment velocity. Predictions are given in parenthesis for TML models having (depleted, solar) abundances. The postmixed gas temperature in the models is $\approx 2 \times 10^5$ K.

^b Radiatively cooling fountain model results from Benjamin 1994. The values are for a gas initially heated to 10^6 K and then allowed to cool over a large range in the quantity $n_H D$ (density times size). The model sets $N(\text{C IV}) \approx 8.4 \times 10^{13}$ cm⁻² in the one-dimensional plane parallel flow. Photoionization effects on Si IV and C IV within the cooling flow are included.

^c The magnetized conductive interface model results are from Borkowski, Balbus, & Fristrom 1990. The values are appropriate for a slice along the front normal and magnetic field inclinations (relative to the conduction front) between 60° and 0° . The conduction front age in the model is 2.5×10^5 yr.

^d Supernova bubble models appropriate for an isolated SN exploding in an ISM having an ambient density of $0.1\text{--}0.3$ cm⁻³ and a magnetic field of $1\text{--}3$ μG (Slavin & Cox 1992). The values are averages over different sight lines through remnants with ages between 4×10^5 and 5×10^6 yr. The ionic ratios listed are similar to those recently calculated by Shelton 1998. However, we note that the actual ratios that would apply for a given situation will depend sensitively on the impact parameter of the line of sight through the evolving remnant.

^e The photoionization calculations of § 5.3 imply that most of the Si IV observed toward μ Col is probably produced in a low-density H II region surrounding the star.

involve nonequilibrium cooling or heating processes. Representative model results are compared with the observations in Table 4. The references for the models are provided in the footnotes of the table. Various heating models involving the nonequilibrium heating of cool gas at conductive interfaces with hot gas predict values of $N(\text{C IV})/N(\text{O VI})$ that are consistent with the observed ratio of 0.11. Moderate-temperature turbulent mixing layer (TML) models predict values of $N(\text{C IV})/N(\text{O VI})$ much larger than observed.

The late evolutionary stages of supernova remnants (SNRs) provide a situation in which the conductive heating model may be appropriate. The supernova (SN) explosion produces hot gas that expands outward and produces an expanding shell of cooler gas. The transition temperature ionization states (e.g., C IV, N V, and O VI) are produced as the cold gas in the postshock shell evaporates into the hot interior of the bubble (see Spitzer 1990). Such models also seem to be capable of explaining the difference in line widths among the various high-ionization lines. For example, Shelton (1998) notes substantial width differences among the C IV, N V, and O VI profiles in the SN evolutionary models that she has calculated. In particular, the model profiles for SN bubbles in their very late stages of evolution bear a strong resemblance to the profiles we see for the μ Col line of sight. It is possible that the sight line is short enough that we are seeing the effects of hot gas absorption

strongly influenced by a single, highly evolved SN event. The range of the expected column density ratios for SN bubbles determined by Slavin & Cox (1992) is given in Table 5. These values are similar to those calculated by Shelton (1998). However, the results for a specific sight line will depend sensitively on the impact parameter of the path through the remnant.

The high-ionization absorption-line column densities toward μ Col may contain a substantial contribution from highly ionized gas situated in the local ISM. The Sun is located near the edge of a small, warm neutral cloud called the Local Cloud, which is contained within a region of unusually hot, low-density gas called the Local Bubble (see Cox & Reynolds 1987). The hot gas in the Local Bubble is probably the source of some of the soft X-ray background (McCammon et al. 1983), and absorption by highly ionized atoms may occur in the interface between the local warm gas and the hot gas of the Local Bubble. Highly ionized gas absorption could also arise in the outer boundary of the local bubble.

Shelton & Cox (1994) have reanalyzed the *Copernicus* O VI data originally presented by Jenkins (1978a, 1978b) and have derived an O VI column density of $\log N(\text{O VI}) \sim 13.2$ that is associated with the Local Bubble. This is within $\sim 40\%$ of the O VI column density predicted for the conductive boundary between the Local Cloud and the Local Bubble by Slavin (1989). The difference is probably not sig-

TABLE 5
GHRS ECHELLE-MODE OBSERVATIONS OF HIGHLY IONIZED INTERSTELLAR ATOMS

Star	MK	l	b	d	z	$\langle n(\text{H I}) \rangle^a$	$\log N(\text{Si IV})$	$\log N(\text{C IV})$	$\log N(\text{N V})$	$\log n(\text{O VI})$	Reference
μ Col	O9.5 V	237.3	-27.1	0.4	0.18	0.057	12.16 ± 0.05	12.88 ± 0.02	11.8–12.3	13.82 ± 0.02	1
γ^2 Vel	O9 I+WC8	262.8	-7.7	0.26	-0.035	0.068	13.05 ± 0.03	13.18 ± 0.03	12.61:	13.71 ± 0.02	2
HD 93521	O9.5 V	183.1	62.2	1.7	1.5	0.024	13.09 ± 0.28	13.63 ± 0.28	...	13.86:	3
HD 119608.....	B1 Ib	320.4	43.1	4.1	2.8	0.061	13.57 ± 0.02	14.48 ± 0.06	13.45 ± 0.07	...	4
ζ Oph.....	O9.5 V	6.3	23.6	0.14	0.015	3.3	12.79 ± 0.02	12.81 ± 0.06	< 12.48 (2 σ)	12.69 (2 σ)	5
HD 167756.....	B0.5 Ia	351.5	-12.3	4.0	-0.85	0.052	13.09 ± 0.02	13.83 ± 0.02	13.56 ± 0.03	...	6
HD 215733.....	B1 II	85.2	-36.4	2.9	-1.7	0.063	13.22 ± 0.08	13.97 ± 0.10	12.29 ± 0.18	...	7

REFERENCES.—(1) This paper; (2) Fitzpatrick & Spitzer 1994; (3) Spitzer & Fitzpatrick 1992; (4) Sembach et al. 1997; (5) Sembach et al. 1994; (6) Savage et al. 1994; (7) Fitzpatrick & Spitzer 1997.

^a The average sight line H I density, $\langle n(\text{H I}) \rangle = N(\text{H I})/d$, is listed. The values of $N(\text{H I})$ are from Diplas & Savage 1994. In the case of ζ Oph, we list $\langle n(\text{H}) \rangle = [N(\text{H I}) + 2N(\text{H}_2)]/d$ with the H I and H₂ column densities from Bohlin et al. 1978.

nificant given the unknown effects of patchiness in the Local Cloud boundary and the viewing geometry of the interface. However, the Shelton & Cox (1994) estimate is about a factor of 4 smaller than the O VI column density toward μ Col, which suggests that some of the O VI along the sight line may occur beyond the Local Bubble. Additional evidence for a more distant origin for some of the O VI comes from GHRS measurements of the C IV absorption toward ϵ CMa by Gry et al. (1995); ϵ CMa is located about 132 pc from the Sun (ESA 1997) in the direction $l = 239^\circ.8$, $b = -11^\circ.3$, about 16° away from the μ Col sight line. Gry et al. (1995) detect two C IV components: one with $v_{\text{HELIO}} = 17$ km s $^{-1}$ and $\log N(\text{C IV}) = 12.51$, and one with $v_{\text{HELIO}} = -10$ km s $^{-1}$ and $\log N(\text{C IV}) = 12.62$. The first component has a velocity that is consistent with that of the Local Cloud for this direction (Lallement & Bertin 1992), and the velocity is nearly identical to that of the C IV absorption toward μ Col. If the local C IV column density at $v_{\text{HELIO}} = 17$ km s $^{-1}$ toward ϵ CMa is representative of the amount toward μ Col, then we conclude that $\sim 40\%$ of the C IV toward μ Col arises within the Local Bubble region. Using a value of $N(\text{C IV})/N(\text{O VI}) \sim 0.18$ for this gas (Slavin 1989) implies that only about 25% of the observed O VI is associated with this gas. This is in good agreement with the general results of the Shelton & Cox (1994) Local Bubble analysis. We conclude that there must be additional sources of C IV and O VI in more distant gas along the sight line toward μ Col and that the absorption may be produced in the hot, collisionally ionized gas associated with an old evolved SNR.

6. DISCUSSION

In this section, we consider how the results for the highly ionized gas absorption toward μ Col fit into the broader context of absorption by highly ionized interstellar gas in the Galactic disk and halo. In their survey of interstellar Si IV, C IV, and N V along Galactic and extragalactic sight lines, Savage et al. (1997) found evidence for substantial variation (up to a factor of 10) in the high ion average sight line densities and ionic ratios. Spitzer (1996) similarly found that $N(\text{C IV})/N(\text{O VI})$ exhibits a factor of 10 variation, with a strong tendency for halo star sight lines to exhibit large ion ratios [$\langle N(\text{C IV})/N(\text{O VI}) \rangle \approx 1.1$] and disk star sight lines to exhibit small ion ratios [$\langle N(\text{C IV})/N(\text{O VI}) \rangle \approx 0.15$]. The ratio $N(\text{C IV})/N(\text{O VI}) = 0.11$ toward μ Col is similar to the disk star result.

The large variations in the integrated high-ionization column density ratios suggest that processes involving a wide range of physical conditions are operating to create the highly ionized gas. An excellent way to separate the varying absorption contributions from gas parcels with different physical conditions is to compare directly

absorption-line profiles obtained at high resolution and high S/N. Table 5 lists those interstellar sight lines for which GHRS echelle-mode (FWHM = 3.5 km s $^{-1}$) observations of the high ions have been obtained. The interstellar lines of sight so far studied include those to nearby stars in the Galactic disk (μ Col, ζ Oph, and γ^2 Vel) and to distant stars sampling gas in the low Galactic halo (HD 93521, 119608, 167756, and 215733). The disk sight lines probe regions of high (ζ Oph) and low (μ Col, γ^2 Vel) neutral hydrogen density, while the halo sight lines are mostly sample regions of low average density. For many of the sight lines listed in Table 5, the detailed profile intercomparisons discussed in the referenced papers reveal the existence of multiple types of highly ionized gas. The narrow absorption components observed in some cases have been attributed to warm photoionized gas (ζ Oph, γ^2 Vel), while in other cases they have been attributed to highly ionized gas in conductive interfaces between the warm and hot ISM (HD 167756). The broad, highly ionized gas absorption seen in O VI, N V, C IV, and occasionally in Si IV provides direct evidence for the existence of hot gas with $T = (1-5) \times 10^5$ K. The relative mix of the interface and coronal gases varies from sight line to sight line. Determining the most common processes for creating these high ions along representative ISM disk or halo sight lines will require the acquisition of high-resolution profiles for a larger number of stars. The high-ionization absorption-line database should improve considerably over the next few years with the availability of the Space Telescope Imaging Spectrograph, which can be used to observe efficiently Si IV, C IV, and N V absorption with two separate integrations in its high-resolution mode (E140H).

Although *HST* observations of N V have proved to be an important tracer of hot, collisionally ionized interstellar gas, the N V $\lambda\lambda 1238.8$ and 1242.8 lines are often very weak and tend to be blended with complex stellar absorption. These complications can make interpretations of the ISM N V absorption difficult. With 114 eV required for its production, O VI stands out as the most important tracer of gas in the temperature regime from 10^5 to 10^6 K. We look forward to the launch of the *Far-Ultraviolet Spectroscopic Explorer* and its potential for observing interstellar O VI $\lambda\lambda 1031.9$ and 1037.6 both in absorption and emission.

This paper is based on observations made with the NASA/ESA *Hubble Space Telescope*, obtained at the Space Telescope Science Institute, which is operated by the Association of Universities for Research in Astronomy, Inc., under NASA contract NAS 5-26555. We very much appreciate the efforts of the many people who contributed to the success of the *HST* and GHRS programs.

REFERENCES

- Anders, E., & Grevesse, N. 1989, *Geochim. Cosmochim. Acta*, 53, 197
 Benjamin, R. A., 1994, Ph.D. thesis, Univ. Texas
 Black, J. H., Dupree, A. K., Hartmann, L. W., & Raymond, J. C. 1980, *ApJ*, 239, 502
 Bohlin, R. C., Savage, B. D., & Drake, J. F. 1978, *ApJ*, 224, 132
 Borkowski, K. J., Balbus, S. A., & Friskrom, C. C. 1990, *ApJ*, 355, 501
 Brandt, J. C., et al. 1993, *AJ*, 105, 831
 ———, 1994, *PASP*, 106, 890
 ———, 1995, *AJ*, 109, 2706
 ———, 1996, *AJ*, 112, 1128
 ———, 1997, *AJ*, 114, 554
 ———, 1998a, *AJ*, 116, 971
 ———, 1998b, *AJ*, submitted
 Brown, A. G. A., Hartmann, D., & Burton, W. B. 1995, *A&A*, 300, 903
 Cardelli, J. A., & Ebbets, D. C. 1994, in *HST Calibration Workshop, Calibrating Hubble Space Telescope*, ed. J. C. Blades & A. J. Osmer (Baltimore: STScI), 322
 Cardelli, J. A., Ebbets, D., & Savage, B. D. 1993, *ApJ*, 413, 401
 Cardelli, J. A., Meyer, D. N., Jura, M., & Savage, B. D. 1996, *ApJ*, 467, 334
 Cowie, L. L., Taylor, W., & York, D. G. 1981, *ApJ*, 248, 528
 Cox, D. P., & Reynolds, R. J. 1987, *ARA&A*, 25, 203
 Diplax, A., & Savage, B. D. 1994, *ApJS*, 427, 274
 ESA. 1997, *The Hipparcos and Tycho Catalogues* (ESA SP-1200) (Noordwijk: ESA)
 Ferland, G. J. 1996, *Hazy*, a Brief Introduction to CLOUDY 90, Univ. Kentucky Phys. Dept. Internal Rep.
 Ferland, G. J., Korista, K. T., Verner, D. A., Ferguson, J. W., Kingdon, J. B., & Verner, E. M. 1998, *PASP*, 110, 761

- Fitzpatrick, E. L. 1997, ApJ, 482, L199
Fitzpatrick, E. L., & Spitzer, L. 1994, ApJ, 427, 232
———. 1997, ApJ, 475, 623
Gry, C., Lemonon, L., Vidal-Madjar, A., Lemoine, M., & Ferlet, R. 1995, A&A, 302, 497
Heap, S. R., et al. 1995, PASP, 107, 871
Hibbert, A., Dufton, P. L., Murray, M. J., & York, D. G. 1983, MNRAS, 205, 53
Howarth, I. D., & Prinja, R. K. 1989, ApJS, 69, 527
Howk, J. C., Savage, B. D., & Fabian, D. 1998, in preparation
Jenkins, E. B. 1978a, ApJ, 219, 845
———. 1978b, ApJ, 220, 107
Kurucz, R. L. 1991, in Proc. Workshop on Precision Photometry, Astrophysics of the Galaxy, ed. A. C. Davis Philip, A. R. Upgren, & K. A. James (Schenectady: Davis), 27
Lallement, R., & Bertin, P. 1992, A&A, 266, 479
Linsky, J. L., et al. 1993, ApJ, 402, 694
———. 1995, ApJ, 451, 335
Mathis, J. S. 1996, ApJ, 472, 643
McCammon, D., Burrows, D. N., Sanders, W. T., & Kraushaar, W. L. 1983, ApJ, 269, 107
Meyer, D. N., Jura, M., & Cardelli, J. A. 1998, ApJ, 493, 222
Mihalas, D., & Binney, J. 1981, Galactic Astronomy (2d ed.; San Francisco: Freeman)
Morris, S. L., Weymann, R. J., Savage, B. D., & Gilliland, R. L. 1991, ApJ, 377, L21
Morton, D. C. 1991, ApJS, 77, 119
Robinson, R. D., et al. 1998, PASP, 110, 68
Savage, B. D. 1987, in Interstellar Processes, ed. D. J. Hollenbach & H. A. Thronson, Jr. (Dordrecht: Reidel), 123
Savage, B. D., Bohlin, R. C., Drake, J. F., & Budich, W. 1977, ApJ, 216, 291
Savage, B. D., & Sembach, K. R. 1991, ApJ, 379, 245
———. 1996, ARA&A, 34, 279
Savage, B. D., Sembach, K. R., & Cardelli, J. A. 1994, ApJ, 420, 183
Savage, B. D., Sembach, K. R., & Lu, L. 1997, AJ, 113, 6
Sembach, K. R., Danks, A., & Savage, B. D. 1993, A&AS, 100, 107
Sembach, K. R., & Savage, B. D. 1992, ApJS, 83, 147
———. 1994, ApJ, 430, 201
Sembach, K. R., Savage, B. D., & Jenkins, E. B. 1994, ApJ, 421, 585
Sembach, K. R., Savage, B. D., & Tripp, T. 1997, ApJ, 480, 216
Shelton, R. 1998, ApJ, 504, 785
Shelton, R., & Cox, D. P. 1994, ApJ, 434, 599
Shull, M., & York, D. G. 1977, ApJ, 211, 803
Slavin, J. D. 1989, ApJ, 346, 718
Slavin, J. D., & Cox, D. P. 1992, ApJ, 392, 131
Slavin, J. D., Shull, J. M., & Begelman, M. C. 1993, ApJ, 407, 83
Snowden, S., et al. 1997, ApJ, 485, 125
Sofia, U. J., Cardelli, J. A., & Savage, B. D. 1994, ApJ, 430, 650
Sofia, U. J., Savage, B. D., & Cardelli, J. A. 1993, ApJ, 413, 251
Spitzer, L. 1990, ARA&A, 28, 71
———. 1996, ApJ, 458, L29
Spitzer, L., & Fitzpatrick, E. L. 1992, ApJ, 391, L41
Sutherland, R. S., & Dopita, M. A. 1993, ApJS, 88, 253
York, D. G. 1974, ApJ, 193, L127